






## 1g Modelling of Lateral Deformation of 2×2 Short Pile Group Foundations in Liquefied Sand

Arief Alihudien<sup>1\*</sup>, As'ad Munawir<sup>2</sup>, Yulvi Zaika<sup>2</sup>, Eko Andi Suryo<sup>2</sup>

<sup>1</sup> Department of Civil Engineering, Brawijaya University, Jember 68121, Indonesia

<sup>2</sup> Department of Civil Engineering, University of Brawijaya Malang, Malang 64145, Indonesia

Corresponding Author Email: [ariefalihudien@unmuhjember.ac.id](mailto:ariefalihudien@unmuhjember.ac.id)

Copyright: ©2024 The authors. This article is published by IETA and is licensed under the CC BY 4.0 license (<http://creativecommons.org/licenses/by/4.0/>).

<https://doi.org/10.18280/mmep.110819>

### ABSTRACT

**Received:** 19 February 2024

**Revised:** 20 June 2024

**Accepted:** 28 June 2024

**Available online:** 28 August 2024

#### **Keywords:**

*shaking table, group pile, lateral deformation*

The earthquake that occurred in Palu-Sulawesi Indonesia in 2018 has caused many problems to infrastructure buildings. One of the impacts of the earthquake was the reduction the level of hardness includes the level of stiffness saturated sandy and condition makes the foundation structure experience greater lateral deformation, which can lead to the collapse of the building above it. This phenomenon is called liquefaction. This article describes the results of laboratory simulations using a one-way shaking table. It aims to obtain the lateral resistance of a group of short pile foundations. The lateral resistance is investigated from the amount of lateral deformation of the pile cap. Laboratory modeling used field and laboratory comparisons at a scale of 1:10. Pile foundations are used in 2×2 pile groups. To obtain the lateral deformation of the pile, Optic Flow is used which is placed on top of the pile cap as high as 30cm. Meanwhile, to obtain the increase in pore water pressure, a PWP sensor was used which was inserted at a certain soil depth of 30cm from the ground surface. The test results show that the lateral deformation of the pile cap due to liquefaction can be observed well. The phenomenon of liquefaction can be observed the excess the pressure of pore water into the soil is caused by loading of seismic. Furthermore, observation results were compared through analysis using the Plaxis 3D program, which showed a good agreement.

## 1. INTRODUCTION

Liquefaction is a transformation process from granular material in solid form to liquid form which is caused by the process of increasing pore water pressure in the soil and the loss of effective stress in the soil. The increase in pore water pressure is due to the tendency of grained materials to compact due to cyclic shear deformations. The 2018 earthquake in Palu, Sulawesi, Indonesia, showed us that soil liquefaction caused by earthquakes has a significant impact on the safety of buildings and human lives. It is necessary to pay close attention to how to maintain our building structures to always withstand liquefaction events, by studying the characteristics of soil and foundation structures when liquefaction occurs.

The behavior of sandy soils undergoing liquefaction due to earthquakes has been studied, including simulation using shaking table tests by several researchers. Pathak et al. [1] have examined the effect of variations in soil density and earthquake vibration acceleration on sand soil resistance to liquefaction using a one-way shaking table test. Chen et al. [2] Using a two-way earthquake-loaded shaking table, the results showed that the use of a two-way shaking table resulted in greater liquefaction potential than a one-way shaking table. Varghese and Madhavi Latha [3] used a one-way shaking table to see soil resistance to liquefaction that varies soil density,

vibration acceleration, and frequency. The behavior of foundations in seismic areas will be significantly affected if soil liquefaction occurs. The stiffness and strength of the soil will decrease as a result of the increase in pore water pressure. Frequent damage to pile foundations during earthquakes has given us insight into the interaction mechanism of pile foundations with soil during liquefaction. In the study conducted by Chen et al. [2], a shaking table was used to observe the effect of soil stiffness reduction due to liquefaction on the lateral deformation of a single pile foundation.

Observations showed an increase in excess pore pressure accompanied by a decrease in soil effective stress. The decrease in soil effective stress will decrease the stiffness and increase the deformation of the pile foundation. In Leblanc [4], a shaking table test was used to investigate the effect of liquefaction on the lateral load of 2×2 pile foundations. Additional lateral load during liquefaction was observed. Haeri et al. [5] has also used a one-way shaking table to observe the response of a group of rigid 3×3 piles to lateral spreading due to liquefaction using as for the 1 g shake table test on a large scale. The soil model can consist of a soil profile with 3 layers: the base layer cannot be liquefied. The middle layer can be liquefied and the top layer cannot be liquefied. The observation results were lateral deformation and additional lateral load on the pile foundation. Next used a

centrifuge shaking table, the behavior of 2×2 rigid pile foundations with pile tips wedged in bedrock due to liquefaction has been observed.

There is still no observation and simulation of lateral resistance of short pile foundation groups due to liquefaction. Short pile foundations are pile foundations whose collapse to lateral loads is dominated by the collapse of soil resistance [6, 7]. The lateral resistance of the foundation can be evaluated from the amount of deformation that occurs when the lateral load acts. Indonesian National Standard 8460 on geotechnical design requirements stipulates that the allowable deformation during an earthquake is 12mm for a planned earthquake and 25mm for a strong earthquake under single-pile and free-head conditions. Prediction of lateral deformation of pile foundations due to earthquake loads in liquefaction soils is very important, in maintaining the stability of the foundation structure. This article describes the results of laboratory

modeling using a one-way shaking table to obtain a description of the lateral and vertical deformation of a 2×2 rigid/short pile foundation group due to liquefaction, as well as the results compared with the analysis using Plaxis 3.

## 2. MATERIALS, TEST EQUIPMENT AND METHODS

### 2.1 Method

This modeling was carried out on a small scale in the laboratory as shown in Figure 1. The scale used was a 1:10 scale. The sequence of work carried out is an assembly of a shaking table, ether sensor, assembly of Pore Water Pressure sensor, assembly of Optic flow sensor, foundation model making, soil sample testing, and simulation of pile foundation behavior in liquefied soil with shaking table, simulation results

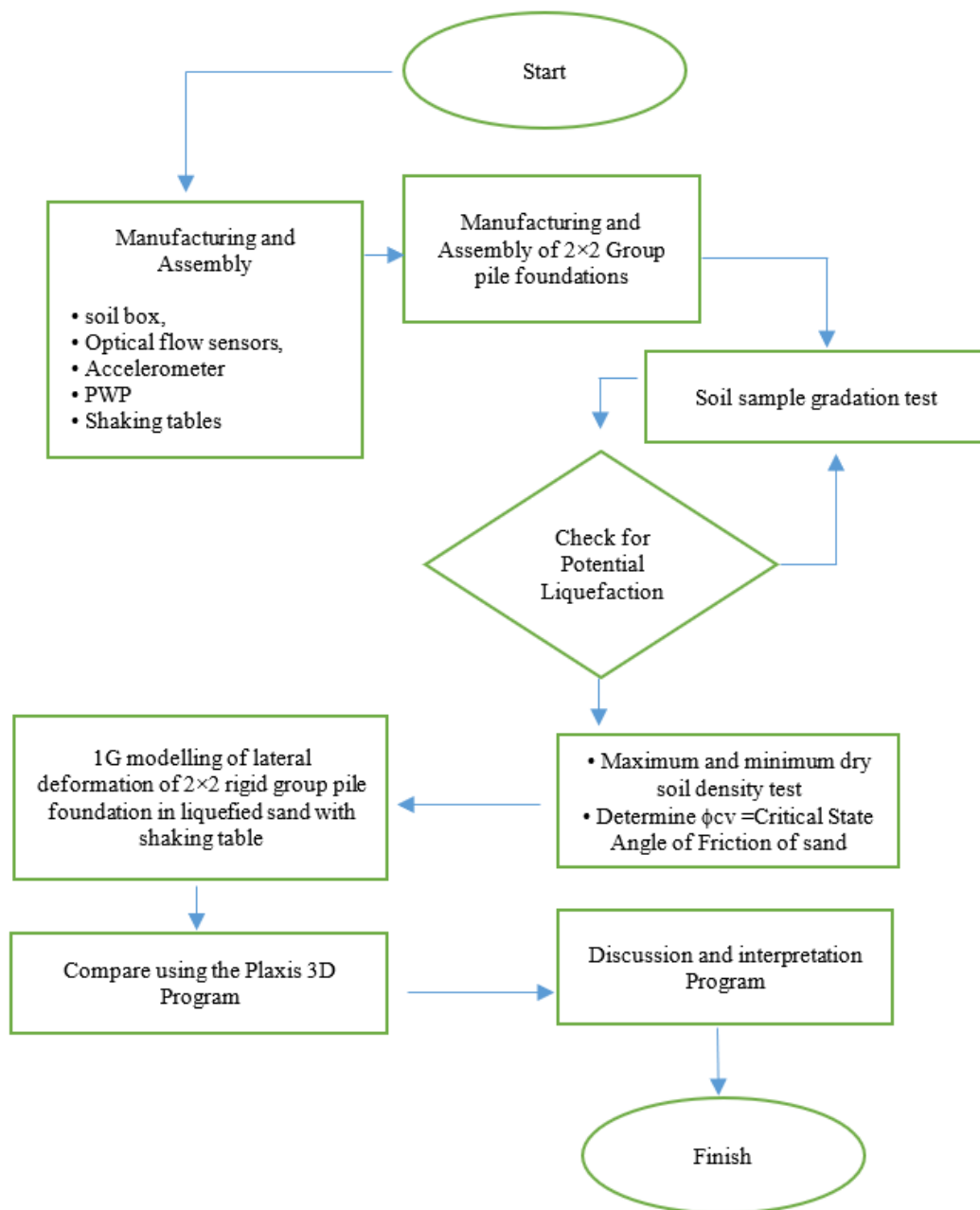


**Figure 1.** Flowchart of 1g modeling of lateral deformation of pile foundation in liquefied soil

## 2.2 Shaking table

The shaking table uses a 2.2kW 1420RPM drive motor. Ground motion input in the form of sinusoidal motion is generated using an electric motor connected to the shaking table through a connecting rod. The motion generated by the electric motor is transmitted to the connecting rod through a pulley. There are 2 pulleys assembled to drive the crankshaft. The motion generation system uses an inverter so that the speed and frequency of the ground motion input can be adjusted automatically. Inverter (VFD) used SHZK brand, Model ZK880-3KW, Input 380V 3 Phase +/- 15% 47-65HZ, Output 380V 3 Phase +/- 15% 47-65HZ 6.8A, Frequency Range 0-600HZ, and Capacity 3KW/4HP.

The amplitude (deviation) of the sinusoidal motion can be adjusted manually by moving the position of the control lever or crankshaft. The sketches of the shaking table and sensor are presented in Figure 2 and Figure 3. For this study the motion input can be represented by developing Eq. (1):

$$x = A \sin(\omega t + \beta) \quad (1)$$

where,  $x$  is the displacement at time  $t$ ,  $A$  is the amplitude,  $\omega$  is the angular frequency of the motion,  $t$  is the time, and  $\beta$  is the initial stage angle in degrees in the sine function.

By adopting Eq. (1), the system movement speed can be determined which is the first derivative of the function, Eq. (2).

$$\dot{x} = A \cdot \omega \cdot \cos(\omega t + \beta) \quad (2)$$

Thus, the acceleration of the system motion can be determined which is the second derivative of the motion function and is expressed in Eq. (3).

$$\ddot{x} = -A \cdot \omega^2 \cdot \sin(\omega t + \beta) \quad (3)$$

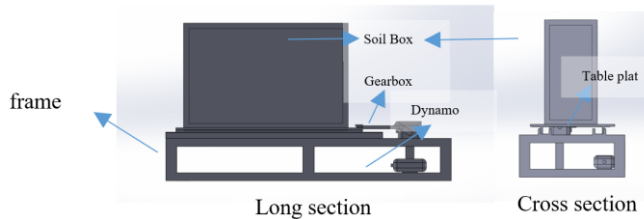


Figure 2. Shaking table schematic



Figure 3. Photo of shaking table and rigid container equipment

## 2.3 Pore water pressure

For the purpose of observing liquefaction behavior in the soil close to the pile, one sensor was installed to observe the increase in pore water stress (PWP), with a depth of 30cm, as in Figure 4.



Figure 4. Soil pore water pressure test equipment

To measure pore of water pressure, the PWP sensor needs to be calibrated. Calibration is done by reading that the PWP sensor is placed in an open space ( $f_0$ ), then compared to the reading placed in the ground without any vibration from the shaking table ( $f_i$ ). This is done to get the value of  $k$  in Eq. (4).

$$P = k(f_0 - f_i) \quad (4)$$

where,  $P$  he estimated pore of water pressure at measured depth,  $k$  (calibration coefficient) sensor pore water pressure measurement. For calibration, measurements were taken at a depth of 0.3m from the groundwater table. After analyzing the reading results, it can be seen that the pore water pressure at a depth of 0.3m is at an average of 2.9KPa.

## 2.4 Accelerometer

To control the earthquake acceleration given just above the shaking table, a smartphone accelerometer was installed. An accelerometer is also installed above the pile cap to obtain the acceleration distributed on the pile cap. Measurement calibration using the smartphone accelerometer is used to predict the maximum acceleration calculated from the amplitude ( $A$ ) and frequency ( $f$ ) applied to the shaking table vibration. The frequency will be read by the inventor. Predicted maximum acceleration is  $a_{mak0} = Aw^2$ . Where  $w$  is the angular velocity. While the acceleration calibration can be used in the equation that  $a_{mak0} = a_n \cdot a_{mak1}$ . Where  $a_{mak0}$  is the maximum predicted acceleration,  $a_{mak1}$  is the acceleration of the accelerometer reading, and  $a_n$  is the acceleration calibration factor. For  $A$  is 0.005m and amplitude is 2 Hz, we get an angular velocity of 12.56 and  $a_{mak0}$  is 0.08g.

## 2.5 Sensor optic flow

Optical flow meter sensors are then installed on top of the group pile model to measure the amount of deformation that occurs in the pile cap. Optical flow sensors are electronic devices used to measure changes in the position of an object or vehicle by observing changes in the light pattern that appears around the object. It works by measuring the difference in light intensity received by the sensor as the object

moves. Optical flow sensors can also read the shifting movement of objects in front of measuring difference in intensity of light received from the surrounding environment. This allows the sensor to detect lateral and vertical movement of the pile cap. The placement of the sensor can be seen in Figure 5.



Figure 5. Placement of optic flow sensor on rigid container

There are several drawbacks to using this sensor including sensitivity to lighting thus it can be inaccurate in low or changing lighting conditions, susceptible to Environmental Interference: Dust, dirt, or other particles can interfere with sensor performance, resolution limitations: (a) optical flow sensors may have resolution limitations, especially in detecting small changes in poorly lit environments; (b) optical flow sensors may have resolution limitations; (c) limitations on Reflective Surfaces: These sensors may experience difficulties on highly reflective surfaces, such as mirrors or

water; (d) resolution limitations: Optical flow sensors may have resolution limitations, especially in detecting small changes in poorly lit environments. This has been overcome by using special programming filters to correct the readings for accuracy. coating the optical flow lens with clear acrylic to protect the sensor from dust, as well as cleaning the acrylic surface before testing, the test room has sufficient lighting, and does not use reflective surfaces on the reading medium.

As with other sensors, the optical flow sensor also needs to be calibrated in its measurements. Optic flow calibration is done by making a simple trial. This simple trial is done by placing the optic flow for a certain height position and then highlighting the object to be moved with a certain length of movement. This trial was carried out for several trials.

## 2.6 Rigid container

The soil box resting on the shaking table is a Rigid Container type, where the wall on the edge is considered rigid. The soil box is made with dimensions of 1500mm long, 300mm wide, and 1000mm high, as presented in Figure 6. The determination of the dimensions of this soil box is based on research carried by Fishman et al. [8] and Maheshwari et al. [9], and who have analyzed the near zone at the end wall exposed to an artificial boundary. The studies that have been carried out have obtained information This zone extends from the end wall into the container at a specified distance of 1.5-2.0 times the height of the container. The ground box material was made of acrylic on all four sides with a thickness of 10mm. At the confluence of the sides, it is connected with steel material.

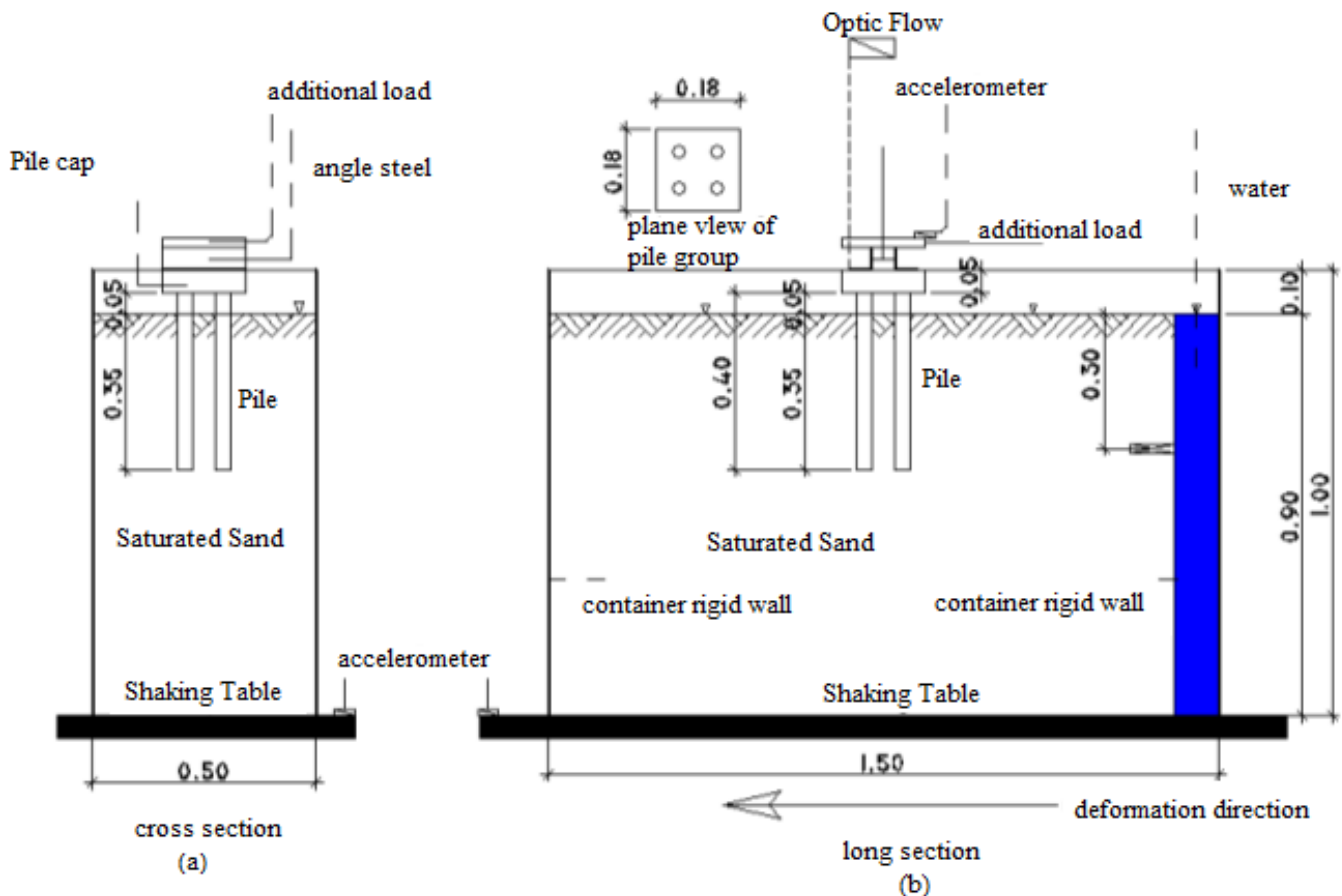


Figure 6. Rigid container model: (a) Cross section; (b) Long section (unit in meters)

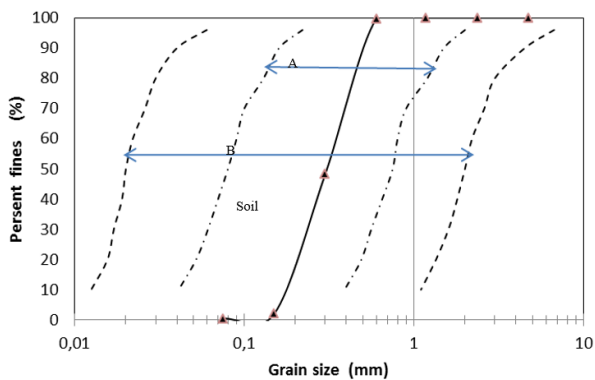
## 2.7 Soil material

The soil material used was sand soil from Puger Beach-Jember Indonesia. Sand soil sampling is done by taking it in disturb conditions. Furthermore, in the laboratory, a gradation test (ASTM D1140), specific gravity test (ASTM D854-14), and Relative density test (ASTM D2049) were conducted. The soil characteristics test results can be shown in Table 1. The soil samples were classified as having potential liquefaction characteristics based on Tsuchida [7], Fourie and Tshabalala [10], and Ishihara [11], soil grain gradation boundaries as shown in Figure 7.

**Table 1.** Soil sample properties

No.	Parameter	Value
1	Effective diameter $D_{10}$	0.18
2	Average diameter $D_{50}$	0.3
3	$D_{30}$	0.18
4	$D_{60}$	0.35
5	Uniformity coefficient $C_u$	1.94
6	Coefficient of gradation $C_c$	1.43
7	Fines contend	0.12
8	PI	NP
9	$\gamma_d$ max	1.379
10	$\gamma_d$ min	1.74
11	$e_{max}$	0.618
12	$e_{min}$	0.104

Source: Laboratory experiment results



(Note: A = boundary of the most liquefying soil and B = boundary of soil that has the potential to experience liquefaction, then it can separate liquefying soil from soil that is not liquefying).

**Figure 7.** The grain size distribution curve for sand originating from Puger Jember includes boundaries in a gradation curve

**Table 2.** Recommendations for determining critical conditions of angel friction from Acta Geotechnica

Soil Property	Determinate From	Classification	Parameter
Angularity of particles	Visual Description	Rounded to well rounded	$\Delta\phi_1=0$
		Subangular to subrounded	$\Delta\phi_1=2$
		Very angular to angular	$\Delta\phi_1=4$
Coefficient of uniformity	Soil Grading	$C_u < 2$	$\Delta\phi_2=0$
		$2 < C_u < 6$	$\Delta\phi_2=2$
		$C_u > 6$	$\Delta\phi_2=4$

Another parameter is the Critical state friction of angel  $\phi_{cs}$ . This parameter is determined using Acta Geotechnica (7). The

Acta Geotechnica standard states that  $\phi_{cs}=30+\Delta\phi_1+\Delta\phi_2$ , where the parameter  $\Delta\phi_1$  is the Angularity of particles from soil properties and the parameter  $\Delta\phi_2$  is Coefficient of uniformity ( $C_u$ ) from soil properties, presented in Table 2, from the formula we assume the angularity of particles are rounded to well rounded and Coefficient of uniformity is smaller than two, then  $\phi_{cs}$  is equal to  $30^\circ$ .

In shallow ground spaces, the level of isotropic stress controlling the studied mechanism is very low, resulting in a higher friction angle, especially when the shear modulus is low when compared to almost the same prototype. Some researchers, such as Bhattacharya et al. [12], Yang et al. [13], Kelly et al. [14], and Leblanc et al. [4], solve this problem by using a method of pouring sand at a lower relative density. Figure 8 has presented information on variations in the peak friction angle ( $\phi'$ ) on the average effective isotropic stress ( $p'$ ) with silica sand material at relatively varied relative densities according to Eq. (5) follows in Bolton's stress dilatancy work.

$$\phi' = \phi_{cs} + 3(R_D - \ln p') - 1 \quad (5)$$

where,  $R_D$  = relative density of sand,  $\phi_{cs}$  = critical state angle of friction of sand, for Puger Jember Indonesia sand used  $30^\circ$  and  $p'$  is Isotropic stress (KPa).

Through this method, the effective prototype stress reaches an average of 155kPa with a relative density of 30% which will be modeled in a laboratory model on a small scale, especially at a stress of 20kPa, the sand must be poured at a relative density of around 20% to ensure that peak of friction angle is equal to  $\phi'=33.9^\circ$ . The use of 20% relative density is taken close to the use of relative density done by Pathak et al. [1] and Chen et al. [2].

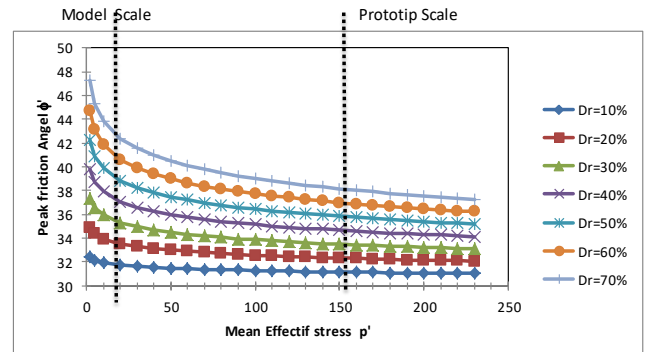


**Figure 8.** Relationship between friction angle, average effective stress, and relative density of Jember Puger sand based on Bolton's stress dilatancy work



**Figure 9.** Compaction trial on rigid box

For compaction with a 20% relative density of the right box, compaction trials were conducted by adjusting the number of passes on a 0.26 KN rolling pin, as shown in Figure 9. These trials were conducted for several relative densities and then a trend was created representing the number of passes and the relative density.

### 2.8 Pile foundation group model

The pile foundation group model is used 2×2, meaning that the foundation consists of 4 foundation piles joined together with a pile cap of concrete, which is presented in Figure 10. The determination of pile depth is based on the notion of short piles (rigid piles) in sandy soil. To get the type of short pile is approximated from the value of  $L < 2T$ , where  $L$  is the depth of the pile into the soil and  $T$  is the modulus of soil stiffness. The modulus of soil stiffness in Eq. (6).

$$T = \sqrt[4]{\frac{EI}{n_k}} \tag{6}$$

where,  $E$  is the modulus of elasticity of the pile,  $I$  is the moment of inertia of the pile, and  $n_k$  is the variation of soil modulus stiffness which can be defined in Table 3

**Table 3.** Values of the Matlock and Resse [15]  $n_k$  soil modulus variations

Soil Type	Loose (KN/m <sup>3</sup> )	Medium (KN/m <sup>3</sup> )	Dense (KN/m <sup>3</sup> )
Dry or moist sand	1800-2000	5500-7000	15000-25000
Submerged sand	1000-1400	3500-4500	8000-12000



**Figure 10.** 2×2 group pile foundation model

The piles in this modeling are used steel pipes with a diameter of  $D=33.6\text{mm}$  and a thickness of  $t=2.6\text{mm}$ . By using the moment of inertia formula  $I = \frac{\pi}{64}(D^4 - (D - t)^4)$ . The absorption includes Carbohydrate Metabolism is  $30,615.57\text{mm}^4$ . The modulus of elasticity of steel material is used  $E=200000\text{N/mm}^2$ . Assuming the pole is in loose soil, then according to Matlock and Resse [15], the soil modulus value used is between 1000-1400. In this modeling, the average soil modulus value  $n_k=1200\text{KN/m}^3$  is used. Thus,

based on the soil modulus stiffness formula,  $T=347.9$  is obtained. If a depth of 1T is used, the depth of the pile foundation is 347.9 mm.

## 3. RESULT AND DISCUSSIONS

An experiment in this article will be presented shaking table simulation using an Amplitude of 5mm. The frequency and Revolution per minute (RPM) used as observed in the inventor readings in Figure 11 and Figure 12. Observations were made within 15 seconds. In this investigation, a speed at an initial frequency of 2Hz or 120RPM was used.

### 3.1 Pore water pressure observation results

As done some previous researchers such as Leblanc et al. [4], Haeri et al. [5], Chen et al. [16], and Liu et al. [17]. To obtain the potential for sand liquefaction, initial observations were made on the increase in pore water tension and excess pore water pressure that occurred in the soil due to the vibration generated. Observations of the increase in pore water pressure are presented in Figure 13 and Figure 14. Figure 13 shows a graph between time and changes in pore water pressure. The average pore water pressure change from the readings is  $7\text{KN/m}^2$ . Figure 14 presents the observation of excess pore water pressure that occurs in the soil due to vibration. The average excess pore water pressure is  $3.5\text{KN/m}^2$ , excess pore of water pressure allows liquefaction in occur. This observation is identical to the liquefaction observations made by Liu et al. [17] using a shaking table at various depths. In conducting the experiment Liu et al. [17] The shaking table is vibrated with an average vibrating acceleration of 0.2g. As for the experiments that have been carried out, the excess pore water pressure obtained at a depth of 0.2m is 2.5KPa, while at a depth of 0.5m is 5KPa. This shows that the investigation conducted which according to the author is close to excess pore water pressure results conducted by Liu et al. [17].

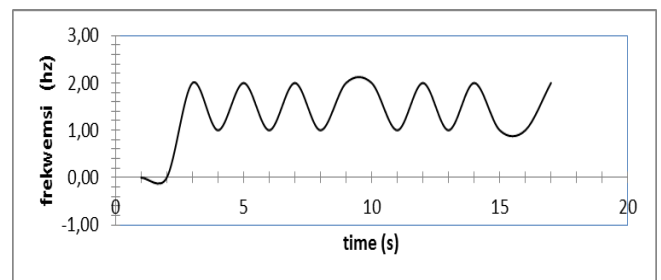


**Figure 11.** Historical time of frequency readings shaking table inventor

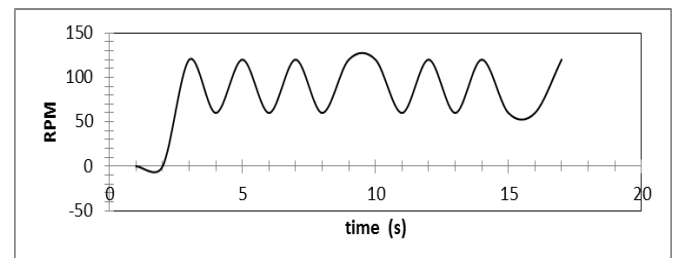


**Figure 12.** Historical time of rpm readings shaking table inventor

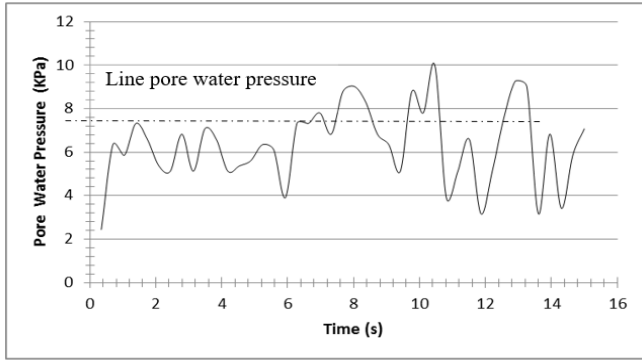


**Figure 13.** Time history of pore water pressure readings in the soil

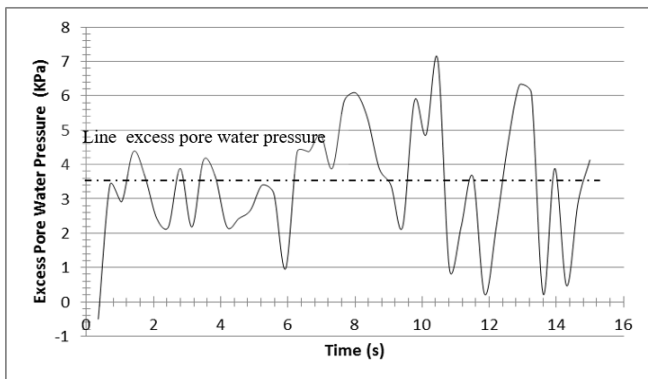


**Figure 14.** Time history of excess pore water pressure readings in the soil

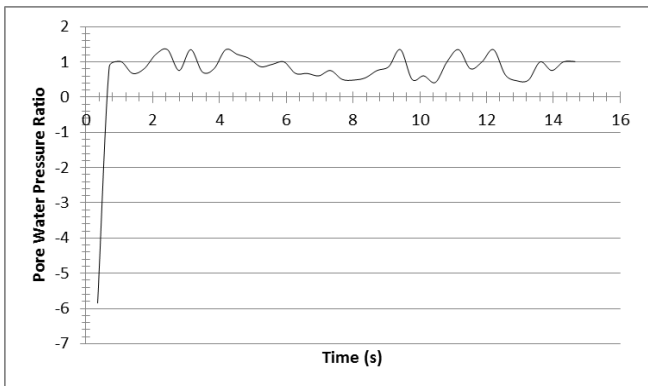


**Figure 15.** Time history of excess pore water pressure ratio

To further explore the liquefaction potential information, we can find the pore water pressure ratio (PPR). The pore water pressure ratio (PPR) is defined in the Eq. (6).

$$PPR = \frac{\Delta P_w}{P'_o} = \frac{P' - P'_o}{P'_o} \quad (7)$$

where,  $\Delta P_w$  is the excess pore water pressure,  $P'$  is the mean effective stress and  $P'_o$  is the initial mean effective stress (i.e. at the beginning of the dynamic analysis). In the case in which the total stress is constant. Varghese and Madhavi Latha [3] have also analyzed the potential for soil liquefaction by obtaining the value of the pore water pressure ratio (PPR). In Figure 15, time history of excess pore water pressure ratio. The graph states that the PPR is about one. This indicates that the soil has a full liquefaction degree.

### 3.2 Accelerometer observation results

Observations of the acceleration of vibration above the shaking table and the pile cap are presented in Figure 16 and Figure 17 and Chen et al [2]. Figure 16 shows the vibration acceleration readings on the shaking table. The acceleration read on the shaking table shows the acceleration of vibration at the bottom of the soil. By the motion input given, the ground at the base is vibrated at a maximum vibration acceleration of 0.08g. The vibration generated at the base of the soil will cause vibrations in the soil and will further cause vibrations in the group pile foundation structure. As a result of the maximum vibration acceleration of 0.08g on the subgrade resulted in a vibration in the pile cap of 0.08g.

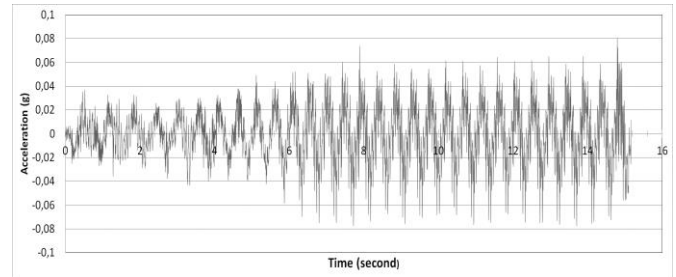


**Figure 16.** Time history of accelerometer readings on shaking table

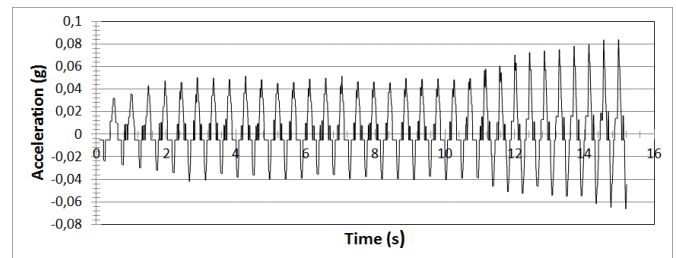


**Figure 17.** Time history of lateral direction accelerometer readings at pile cap

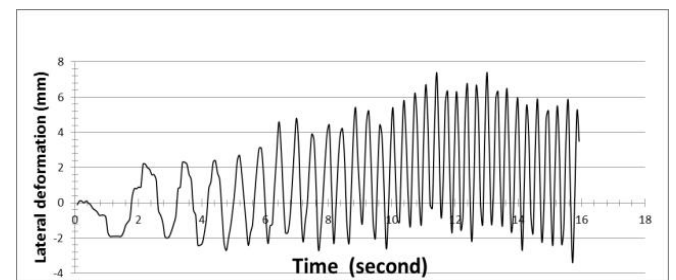


**Figure 18.** Time history of deformation lateral readings on the pile cap

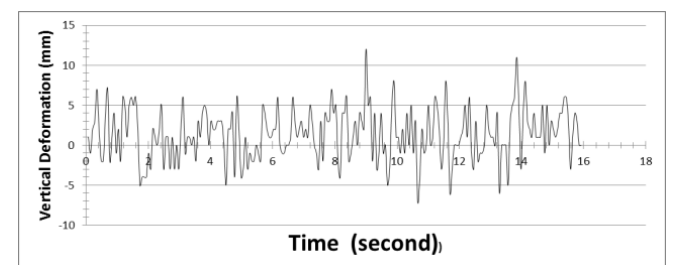


**Figure 19.** Time history of deformation vertical readings on the pile cap

### 3.3 Optical flow observation results

Optic flow is responsible for observing the vertical and lateral movement of the pile cap. These observations are presented in Figure 17 and Figure 18. These observations were also made by Chen et al. [2] to obtain the amount of displacement at the top end of the pile foundation. Figure 17 observes the lateral deformation of the pile cap, while Figure 19 the vertical deformation of the pile cap. The lateral vibration acceleration of the subgrade of 0.08g causes a maximum lateral deformation of the pile cap of 6mm. For vertical deformation of the pile cap due to lateral vibration at an acceleration of 0.08g on the subgrade, it is found to be 12mm.

### 3.4 Discussion of observation results

Validation of the observations can be done by comparing using the finite element method (FEM) program, as has been done by Galavi et al. [18] and Matlock and Reese [15] on the evaluation of a quay wall in the Kobe region of Japan. The finite element method program uses Plaxis 3D with a constitutive model formulation, referred to as UBC3D-PLM. This main aspect of the numerical an approach can be describing terms of a velocity of based two-step formulation, where velocity solid of phase in principle unknown, velocity calculated momentum in conservation equation the water or sand of water and mixture, equation is:

$$\begin{aligned} \rho_w \frac{dv_{w,i}}{dt} &= \frac{\partial p}{\partial x_i} - \rho_w g_i - \frac{n\gamma_w}{k_i} (v_{w,i} - v_{s,i}), \\ (1-n)\rho_s \frac{dv_{s,i}}{dt} &= -n\rho_w \frac{dv_{w,i}}{dt} + \frac{\partial \sigma_{i,j}}{\partial x_j} - \rho_{sat} g_i \end{aligned} \quad (8)$$

where,  $\rho_w$  = density of water,  $v_{w,i}$  = component the water in phase velocity vector direction  $i$ ,  $p$  is defined as pore of water pressured,  $g_i$  = the component the gravitational of acceleration direction  $i$ ,  $n$  = porosity,  $\gamma_w$  = as unit weight of fluid,  $k_i$  = hydraulic conductivity of the soil in direction  $i$ ,  $v_{s,i}$  = the velocity vector component of the solid phase in direction  $i$ ,  $\rho_s$  = density of solid in phase,  $\sigma_{ij}$  = total stress of tensor, and  $\rho_{sat}$  = the saturated of density.

The input parameters that can be used in Model UBC3D-PLM is presented in Table 4 [18]. Generally, these parameters are defined according to laboratory experiments and are in accordance with the parameters required by adjusting the experimental curve in the laboratory.

The soil characteristics and foundation structures used in this modeling can look at Table 5 and Table 6, foundation structure consists a pile cap and a pile foundation. The pile cap structure in Plaxis 3D uses plate material, while the pile foundation structure modeling in Plaxis 3D uses embedded pile material (Figure 20 and Figure 21). The ground motion input in the modeling used a surface displacements facility and selected dynamic displacements for amplitude 0.005m and frequency 2Hz. Figure 22, Figure 23, and Figure 24 are images of the behavior of pore water stress in soil. Figure 22 expresses the excess pore pressure around the pile group foundation. Figure 23 is a time-historical graph of excess pore water pressure at a depth of 400mm. Figure 24 shows the historical time graph of the pore water pressure ratio at a depth of 400 mm and 700mm, increase pore of water stress due vibration is trigger for the soil liquefaction process because the increase in pore water pressure will be accompanied by a decrease in soil effective stress. when the soil experiences a decrease in

effective stress, the shear strength of the soil decreases. The decrease in shear strength will result in a decrease in soil strength and stiffness. The exact condition of soil liquefaction will be indicated by the Pore Water Pressure Ratio value. The 3D Plaxis results show that the Pore Water Pressure Ratio value at a depth of 400mm is 0.8, close to the observations from small-scale laboratory experiments. This can be related to the accuracy of the sensor and soil conditioning. Soil conditioning can be in the form of the level of density and saturation of the soil. from the Pore Water Pressure Ratio graph at a depth of 600mm is 4.3, from this, it can be described that up to a depth of 600mm liquefaction still occurs. A comparison of results using a laboratory scale and finite element method analysis is shown in Table 7. The table shows that the laboratory and finite element method results are not the same but are close.

**Table 4.** Soil characteristics for modeling in the finite element method program

Parameters	Unit	Description
$\phi^p$	(degrees)	Peak friction angle
$\phi^{cv}$	(degrees)	Friction angle at constant volume
$c'$	(stress)	Effective cohesion
$k^e_B$	(-)	Elastic bulk modulus number
$k^e_G$	(-)	Elastic shear modulus number
$k^p_G$	(-)	Plastic shear modulus number
$Nk$	(-)	Power for stress dependency of elastic bulk modulus
$Ng$	(-)	Power for stress dependency of elastic shear modulus
$R_f$	(-)	Power for stress dependency of plastic shear modulus
$P_A$	(stress)	Failure ratio
$fac_{dens}$	(-)	Reference stress
$fac_{post}$	(-)	Fitting parameter to adjust densification rule
$(N_i)_{60}$	(-)	Corrected SPT blow counts

**Table 5.** Soil characteristics for modeling in the finite element method program

Parameters	Unit	R20%
$\gamma_{unsat}$	KN/m <sup>3</sup>	19.8
$\gamma_{sat}$	KN/m <sup>3</sup>	19.8
$\phi$		33.95
$c'$	KN/m <sup>3</sup>	0
$E_{ref}$	KN/m <sup>2</sup>	3,896.7
$\mu$		0.3
$E_{oed}$	KN/m <sup>2</sup>	4762
$G$	KN/m <sup>2</sup>	1361
$K_{w,ref/n}$	KN/m <sup>2</sup>	132700

**Table 6.** Characteristics of foundation structures for modeling in the finite element method program

Parameter	Unit	Nilai
a. Pile Cap		
Thick	M	0.05
Modulus Elasticity	KN/m <sup>2</sup>	21019039
Unit Weight	KN/m <sup>3</sup>	24
b. Pile Foundation		
Foundation Type		Circular Tube
Diameter	M	0.0336
Thick	M	2.600E-3
Modulus Elasticity	KN/m <sup>2</sup>	200000000
Unit Weight	KN/m <sup>3</sup>	78.50
Modulus Geser	KN/m <sup>2</sup>	80000000



**Table 7.** Comparison of results using laboratory scale and finite element method analysis

Parameter	Laboratory	FEM
Excess Pore Pressure maximum (Kpa) Depth=0.4m	3.5	2.8
Excess Pore Pressure maximum (Kpa) Depth=0.7m		22
2Excess Pore Pressure Ratio maximum (Depth=0.4m)	1	0.8
Excess Pore Pressure Ratio maximum (Depth=0.7m)		4.3
$a_{max}$ pile Cap (g)	0.08	<b>0.0007</b>
Lateral Deformation of Pile cap (mm)	6	<b>0.0007</b>
Vertical Deformation of Pile cap (mm)	12	<b>0.1482798</b>

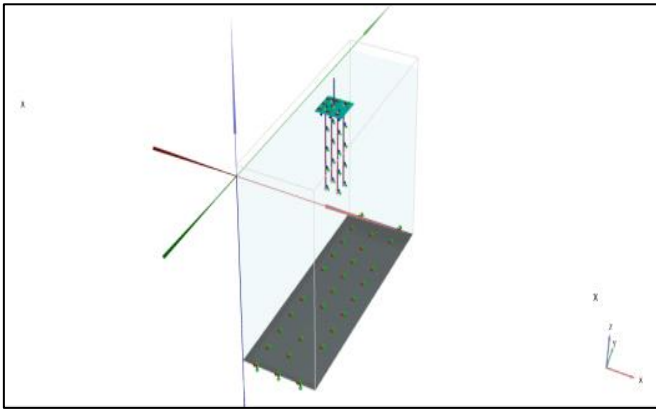


**Figure 20.** 3D Plaxis group pile foundation structure modelling

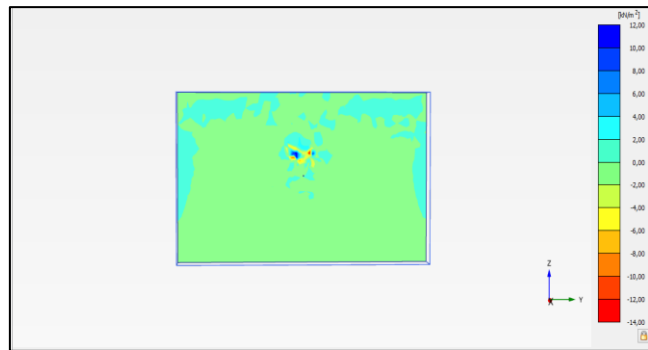


**Figure 21.** Excess pore water pressure around the foundation

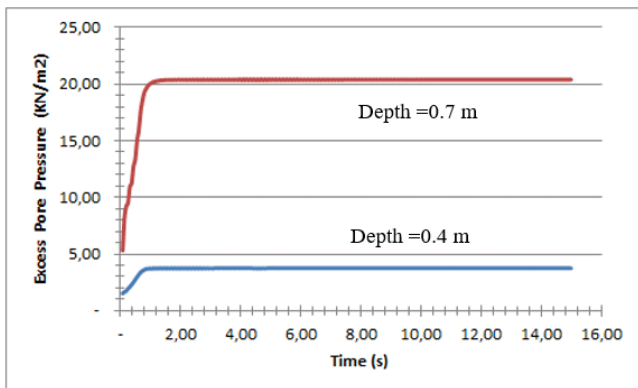


**Figure 22.** Chart time history excess pore water pressure at depth 400 mm

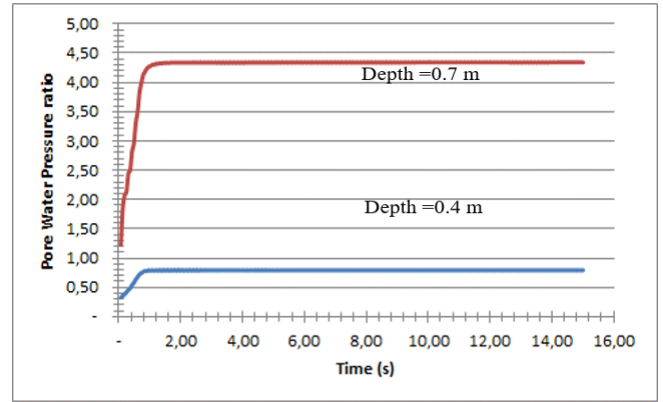


**Figure 23.** Chart time history pore water pressure ratio at depth 400mm

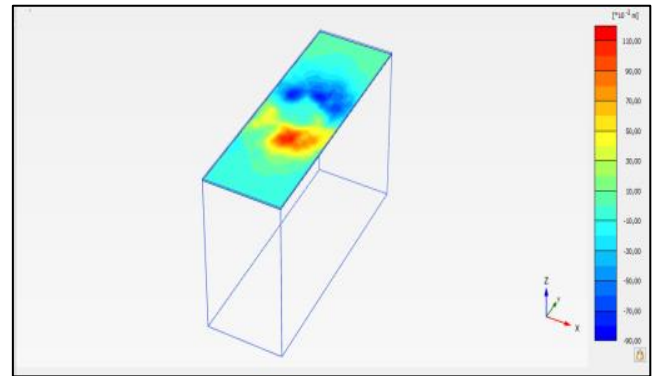


**Figure 24.** Lateral deformation of ground surface

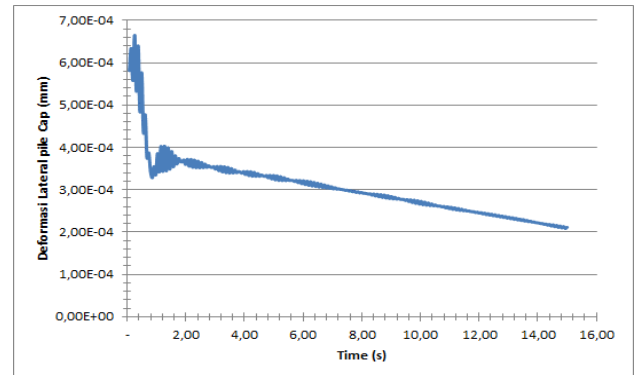


**Figure 25.** Chart time historical deformation lateral at pile cap

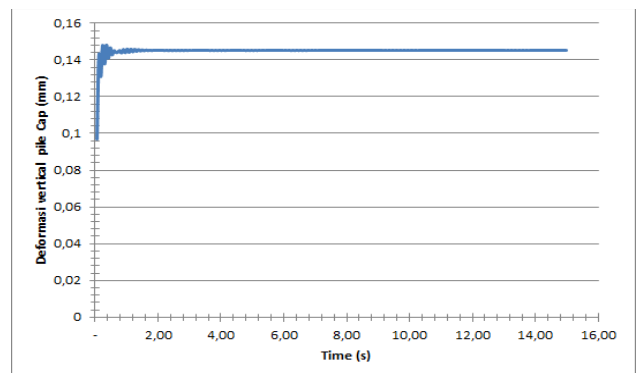


**Figure 26.** Chart time historical deformation vertical at pile cap

Figure 25 shows the time histories of lateral displacement of the pile cap. From the observation, the maximum lateral displacement is 0.0007mm. These results when compared to the experimental observations still appear deviations. Another thing that needs attention is the time histories of lateral deformation until the first second increases, then in the next few seconds the lateral deformation decreases. Figure 26 shows this time histories the vertical displacement pile. From observation, maximum vertical displacement is 0.1482mm. These results when compared with experimental observations still appear deviations. Deviations that occur from observations and 3D Plaxis analysis can occur due to the accuracy of the sensor or soil density that has not been met according to plan. Another thing that needs attention is the time history of lateral deformation until the first second increases, then in the next few seconds the lateral deformation decreases, in contrast to the results of experimental observations in the laboratory conducted by the author. For the experimental observation results shown in Figure 18, the lateral deformation tends to increase, similar to the research conducted by Chen et al. [16].

Figure 23 is an image of lateral in movement count soil above surface of analysis results using the Plaxis 3D program. No observations have been made in the laboratory experiments. The lateral movement will automatically increase the lateral load acting on the pile foundation, which may increase the amount of lateral deformation. Haeri et al. [5] refers to this as lateral spreading.

The addition of lateral deformation is also possible due to the large vertical load acting on the foundation, the greater the vertical load acting on the foundation, the greater the lateral load. Referring to the previous paragraph, it can be said that the evaluation pile of response the spreading of lateral due to liquefaction an important of step toward the design at foundations of pile that are resistant to the destructive phenomenon of lateral spreading due to liquefaction. From this description, it is necessary to optimize the design of the planned pile foundation concerning the possibility of soil liquefaction due to the earthquake. This is done by adjusting the depth, dimensions, vertical load acting on the foundation, earthquake acceleration, and foundation arrangement in the group. Another option is to make the foundation design avoid short piles, which requires further research.

The 1g modeling in the lateral displacement investigation due to liquefaction done by the author certainly has some limitations that need to be observed. It is related to the sensors and ground boxes used. As in the optic flow sensor, PWP Sensor, and Accelerometer Sensor, all sensors must be well calibrated. For the ground box, if a rigid wall is used, the length must be sufficient to anticipate the vibration reflection. 1g modeling is related to the prototype modeled there is a problem of soil stress that is not the same as the prototype, this needs to be considered so that in conducting experiments we will get less than optimal results. This can be used as a test tool using a centrifuge model as done. The use of Plaxis 3D in the context of validating 1g modeling test results is very necessary to obtain an appropriate reference for the 1g modeling test results. This research used a 1g scale model, of course, it will be necessary to be able to predict how the prototype's condition will be. It can be used Muir Wood modeling scale [11, 19]. We can estimate the values of the maximum lateral deformation and the maximum vertical deformation occurring in the prototype under the same earthquake load as shown in Table 8.

**Table 8.** Comparison of prototype and 1g scale factors (laboratory) Muir Wood [19]

Quantity	Scale Factor	
	Prototype	1g (Laboratory)
Length	$n_l$	$1/n$
Mass density	$n_\rho$	1
Acceleration	$n_g$	1
Stress	$n_l n_\rho n_g$	$1/n$
Stiffness	$nG$	$1/n\alpha$
Force	$n_\rho n_g n_l^3$	$1/n^3$
Force/Unit length	$n_\rho n_g n_l nG$	$1/n^2$
Strain	$n_\rho n_g n_l^2 nG$	$1/n(1-\alpha)$
Displacement	$n_\rho n_g n_l^2 nG$	$1/n(2-\alpha)$

#### 4. CONCLUSIONS

This article provides an overview of the use of the 1g scale laboratory modeling method for the behavior of the 2x2 pile foundation group and has been compared with the analysis using the Plaxis 3D program. From the description in this article, it can be conveyed that soil modeling on a laboratory scale can be done well although the results are not the same or there are still deviations. Simulation of earthquake loads that cause soil liquefaction using a shaking table can be observed using pore water pressure installed in the soil. The lateral and vertical deformation of the pile cap can be recorded well through the installation of an optic flow sensor on top of the pile cap. Further research can be done by adjusting the depth of the foundation, the number of formations in the group, the vertical load on the foundation, and the earthquake acceleration, to get a picture of the lateral resistance of the pile foundation model when liquefaction occurs.

#### ACKNOWLEDGMENT

The research supported by Study in Postgraduate Brawijaya University and Civil Engineering Laboratory of Muhammadiyah University of Jember. Technical support in the design of table of shaking table, manufacture the Rigid Box of Container by engineers at the Mechanical Engineering Laboratory, Muhammadiyah University of Jember, would like to express our deepest gratitude.

#### REFERENCES

- [1] Pathak, S.R., Kshirsagar, M.P., Joshi, M.S. (2013). Liquefaction triggering criterion using shake table test. *International Journal of Engineering and Technology*, 5: 4439-4449.
- [2] Chen, C.H., Ueng, T.S., Chen, C.H. (2012). Shaking table tests on model pile in saturated sloping ground. In the 15th World Conference on Earthquake Engineering, pp. 24-28.
- [3] Varghese, R.M., Madhavi Latha, G. (2014). Shaking table tests to investigate the influence of various factors on the liquefaction resistance of sands. *Natural Hazards*, 73: 1337-1351. <https://doi.org/10.1007/s11069-014-1142-3>
- [4] Leblanc, C., Byrne, B.W., Houlsby, G.T. (2010). Response of stiff piles to random two-way lateral loading. *Géotechnique*, 60(9): 715-721.

- <https://doi.org/10.1680/geot.09.T.011>
- [5] Haeri, S.M., Kavand, A., Asefzadeh, A., Rahmani, I. (2013). Large scale 1-g shake table model test on the response of a stiff pile group to liquefaction induced lateral spreading. In Proceedings of the 18th International Conference on Soil Mechanics and Geotechnical Engineering, Paris, France, pp. 919-922.
- [6] Committee on Soil Dynamics of the Geotechnical Engineering Division. (1978). Definition of terms related to liquefaction. *Journal of the Geotechnical Engineering Division*, 104(9): 1197-1200. <https://doi.org/10.1061/AJGEB6.0000688>
- [7] Tsuchida, H. (1970). Evaluation of liquefaction potential of sandy deposits and measures against liquefaction induced damage. (in Japanese). In Proceedings of the Annual Seminar of the Port and Harbour Research Institute, 3: 3-33.
- [8] Fishman, K.L., Mander, J.B., Richards Jr, R. (1995). Laboratory study of seismic free-field response of sand. *Soil Dynamics and Earthquake Engineering*, 14(1): 33-43. [https://doi.org/10.1016/0267-7261\(94\)00017-B](https://doi.org/10.1016/0267-7261(94)00017-B)
- [9] Maheshwari, B.K., Nath, U.K., Ramasamy, G. (2008). Influence of liquefaction on pile-soil interaction in vertical vibration. *ISET Journal of Earthquake Technology*, 45(1): 1-13.
- [10] Fourie, A.B., Tshabalala, L. (2005). Initiation of static liquefaction and the role of  $K_0$  consolidation. *Canadian Geotechnical Journal*, 42(3): 892-906. <https://doi.org/10.1139/t05-026>
- [11] Ishihara, K. (1993) Liquefaction and flow failure during earthquakes. *Géotechnique*, 43(3): 351-451. <https://doi.org/10.1680/geot.1993.43.3.351>
- [12] Bhattacharya, S., Lombardi, D., Dihoru, L., Dietz, M.S., Crewe, A.J., Taylor, C.A. (2012). Model container design for soil-structure interaction studies. In *Role of Seismic Testing Facilities in Performance-Based Earthquake Engineering: SERIES Workshop*, Springer Netherlands, pp. 135-158. [https://doi.org/10.1007/978-94-007-1977-4\\_8](https://doi.org/10.1007/978-94-007-1977-4_8)
- [13] Yang, J., Luo, X.D. (2018). The critical state friction angle of granular materials: Does it depend on grading? *Acta Geotechnica*, 13: 535-547. <https://doi.org/10.1007/s11440-017-0581-x>
- [14] Kelly, R.B., Houlsby, G.T., Byrne, B.W. (2006). A comparison of field and laboratory tests of caisson foundations in sand and clay. *Géotechnique*, 56(9): 617-626. <https://doi.org/10.1680/geot.2006.56.9.617>
- [15] Matlock, H., Reese, L.C. (1962). Generalized solutions for laterally loaded piles. *Transactions of the American Society of Civil Engineers*, 127(1): 1220-1248. <https://doi.org/10.1061/TACEAT.0008439>
- [16] Chen, C.H., Ueng, T.S., Ko, Y.Y. (2015). Changes of pile behavior in liquefiable soil during liquefaction process under 1g shaking table test. In 6th International Conference on Earthquake Geotechnical Engineering, pp. 1-4.
- [17] Liu, C., Tang, L., Ling, X., Deng, L., Su, L., Zhang, X. (2017). Investigation of liquefaction-induced lateral load on pile group behind quay wall. *Soil Dynamics and Earthquake Engineering*, 102: 56-64. <https://doi.org/10.1016/j.soildyn.2017.08.016>
- [18] Galavi, V., Petalas, A., Brinkgreve, R.B.J. (2013). Finite element modelling of seismic liquefaction in soils. *Geotechnical Engineering Journal of the SEAGS & AGSSEA*, 44(3): 55-64.
- [19] Muir Wood, D. (2004). *Geotechnical Modelling*. CRC Press, London. <https://doi.org/10.1201/9781315273556>